STAR CLUSTERS IN A SAMPLE OF BCDS: CHARACTERIZING THE YOUNG STELLAR POPULLATION

Ismael M. Delgado[1], Casiana Muñoz-Tuñón[1], L.M. Cairós[2] and Guillermo Tenorio-Tagle[3]

(1) Instituto de Astrofísica de Canarias (2) Astrophysikalisches Institut Postdam (3) Instituto Nacional de Astrofísica, Optica y Electrónica

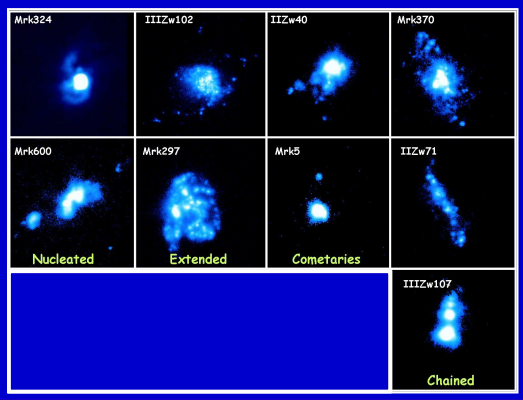
INTRODUCTION AND GOALS

Blue Compact Dwarf (BCD) galaxies are low-luminosity and compact objects, with HII regions-like spectra (Thuan & Martin 1981), low metallicities and high star-forming rates - implying a gas exhaustion timescale shorter than the Hubble time. Initially it was hypothesized that BCDs could be truly young galaxies (Sargent & Searle 1970, Kunth & Sargent 1986). In the last years, extended, redder halos have been detected in the vast majority of them, revealing that, in most cases, BCDs are old systems with recurrent star formation episodes (Loose & Thuan 1986, Telles 1995, Papaderos et al. 1996, Cairós et al. 2001ab, 2002).

We are carrying out a detailed photometric analysis of 9 BCDs, based on a strategy that combines Ha narrow line and broad-band UBVRI photometry. Our goals are:

1) To characterize the young stellar populations: identifiying the star-forming regions and generating a narrow band catalogue which contains the: size, flux, luminosity, SFRs, surface brightnes, EW, the diffuse light emission and the net flux (without diffuse contribution) of every knot.

2) To characterize the actual star formation episode (IMF, age, metallicity, star-forming rate)



THE SAMPLE

The objects have been selected from the sample of Cairós et al. (2001a) belonging to the four categories defined in Cairós etal. (2001b)

PROPERTIES OF THE SAMPLE

1) Different morphology
2) Wide range of luminosities: $-15.5 \geq M_B \geq -20.7$
3) Range of Metallicity: $1/3 \leq Z/Z_O \leq 1/10$
4) Deep photometry
5) Good seeing ~1 "

Hα AND UBVRI PHOTOMETRY: CHARACTERIZING THE YOUNG STELLAR POPULATION

Table 4. *Mrk370 Narrow Band Catalogue*

ID (1)	$\Delta\alpha(")$ (2)	$\Delta\delta(")$ (3)	$R(")$ (4)	$I(pc)$ (5)	$F_{H\alpha}$ (6)	$L_{H\alpha}$ (7)	SFR (8)	SB (9)	EW(Hα) (10)	S/N (11)	F_{net} (12)	F_{diff} (13)
1	0.0	0.0	2.79	146.71	360.59 ± 71.59	$39.79^{+0.06}_{-0.06}$	0.04 ± 0.01	$34.87^{+0.03}_{-0.03}$	188.88	551.00	396.05	39.95
2	-6.4	-3.7	2.34	122.85	145.78 ± 37.46	$39.26^{+0.11}_{-0.12}$	0.02 ± 0.00	$34.63^{+0.05}_{-0.05}$	333.97	351.00	116.60	27.18
3	2.1	-7.4	1.82	95.68	92.80 ± 18.24	$38.64^{+0.08}_{-0.08}$	0.00 ± 0.00	$34.29^{+0.05}_{-0.05}$	223.49	193.00	20.60	12.26
4	-3.2	5.3	1.98	58.71	30.94 ± 33.31	$38.64^{+0.46}_{-0.72}$	0.00 ± 0.00	$34.63^{+0.16}_{-0.16}$	81.03	103.00	25.40	5.55
5	-9.5	27.0	1.98	104.84	7.17 ± 2.44	$38.09^{+0.15}_{-0.18}$	0.00 ± 0.00	$33.47^{+0.05}_{-0.05}$	177.00	64.00	8.81	-1.14
6	19.2	-32.3	2.43	127.78	5.66 ± 0.76	$37.99^{+0.06}_{-0.06}$	0.00 ± 0.00	$33.19^{+0.01}_{-0.01}$	260.79	49.00	5.76	-0.09
7	-17.8	32.0	1.98	104.84	4.92 ± 2.03	$37.94^{+0.15}_{-0.18}$	0.00 ± 0.00	$33.39^{+0.05}_{-0.05}$	189.21	40.00	4.28	0.67
8	-14.3	-9.5	1.43	75.43	4.79 ± 3.16	$37.93^{+0.24}_{-0.30}$	0.00 ± 0.00	$33.57^{+0.08}_{-0.08}$	96.81	54.00	1.22	3.57
9	1.1	8.8	0.90	47.19	4.76 ± 8.84	$37.93^{+0.81}_{-1.94}$	0.00 ± 0.00	$33.98^{+0.14}_{-0.14}$	74.67	60.00	2.00	2.67
10	-12.2	23.8	1.77	93.05	4.58 ± 2.37	$37.81^{+0.17}_{-0.21}$	0.00 ± 0.00	$33.37^{+0.06}_{-0.06}$	133.56	49.00	5.00	-0.42
11	7.9	-28.1	2.67	140.69	3.34 ± 1.11	$37.67^{+0.14}_{-0.16}$	0.00 ± 0.00	$32.87^{+0.03}_{-0.03}$	75.78	30.00	5.72	-2.38
12	-5.8	22.8	2.01	105.51	3.13 ± 1.18	$37.64^{+0.16}_{-0.19}$	0.00 ± 0.00	$33.15^{+0.04}_{-0.04}$	49.05	34.00	4.06	-0.93
13	6.9	1.6	0.95	49.74	1.89 ± 2.56	$37.43^{+0.52}_{-0.96}$	0.00 ± 0.00	$33.53^{+0.16}_{-0.16}$	47.32	35.00	0.00	1.89
14	14.3	-7.9	1.77	93.05	1.76 ± 1.03	$37.39^{+0.26}_{-0.36}$	0.00 ± 0.00	$32.99^{+0.05}_{-0.05}$	79.68	23.00	1.81	-0.03
15	-19.1	3.3	1.81	84.70	1.39 ± 0.94	$37.29^{+0.27}_{-0.36}$	0.00 ± 0.00	$32.94^{+0.06}_{-0.06}$	39.07	20.00	1.74	-0.35
16	2.6	-18.5	1.55	81.73	1.36 ± 1.20	$37.28^{+0.32}_{-0.46}$	0.00 ± 0.00	$32.95^{+0.07}_{-0.07}$	62.01	20.00	0.94	0.51
17	-13.2	32.9	1.12	58.85	1.20 ± 1.14	$37.23^{+0.36}_{-0.54}$	0.00 ± 0.00	$33.19^{+0.05}_{-0.05}$	153.94	22.00	1.04	0.16
18	-5.3	-17.5	1.66	87.59	1.04 ± 1.16	$37.16^{+0.40}_{-0.64}$	0.00 ± 0.00	$32.78^{+0.06}_{-0.06}$	28.84	16.00	0.00	1.04
19	2.1	-22.6	1.27	69.79	0.64 ± 1.06	$36.96^{+0.52}_{-1.06}$	0.00 ± 0.00	$32.81^{+0.09}_{-0.09}$	66.07	12.00	1.54	-0.91
20	7.4	-20.1	1.46	80.62	0.55 ± 1.24	$36.88^{+0.70}_{-1.46}$	0.00 ± 0.00	$32.81^{+0.09}_{-0.09}$	71.01	11.00	0.48	0.07
21	-30.2	19.2	1.28	64.85	0.44 ± 0.46	$36.79^{+0.51}_{-0.96}$	0.00 ± 0.00	$32.67^{+0.05}_{-0.05}$	80.87	9.00	0.36	0.08
22	-22.3	17.0	1.12	58.85	0.37 ± 0.51	$36.71^{+0.56}_{-1.06}$	0.00 ± 0.00	$32.67^{+0.05}_{-0.05}$	58.48	8.00	0.03	-0.16
23	-17.0	30.1	1.04	54.49	0.36 ± 0.69	$36.69^{+0.67}_{-1.67}$	0.00 ± 0.00	$32.72^{+0.06}_{-0.06}$	39.20	8.00	0.28	0.08
24	-18.5	17.5	0.95	44.49	0.21 ± 0.55	$36.46^{+0.91}_{-2.91}$	0.00 ± 0.00	$32.66^{+0.06}_{-0.06}$	39.92	6.00	0.20	0.01
25	-12.7	17.5	0.95	49.74	0.17 ± 0.64	$36.38^{+1.04}_{-3.44}$	0.00 ± 0.00	$32.49^{+0.11}_{-0.11}$	36.03	4.00	0.00	0.17

[1]Col 1: Identification number of each *HII* region catalogued, see Fig.3. Cols. 2,3: Relative coordenates to the brightest knot; Cols. 4,5: Radius; Cols. 6: Total flux in $H\alpha$ for each knot; Col. 7: Luminosity($erg \cdot s^{-1}$) in $H\alpha$ in logarithmic scale; Col. 8: *SFR* in $M_\odot \cdot yr^{-1}$; Col. 9: Surface brightness ($erg \cdot s^{-1} \cdot pc^{-2}$) in logarithmic scale; Col. 10: Equivalent width in $H\alpha$; Col. 11: Signal to noise ratio; Col. 12: Net flux in $H\alpha$, without the diffuse emission contribution; Col. 13: Diffuse emission flux in $H\alpha$. Fluxes are in $10^{-16} erg \cdot s^{-1} \cdot cm^{-2}$ units.

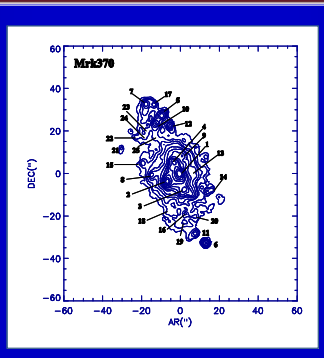


Table 5. *Broad Band Catalogue of Mrk370*

ID (1)	m_U (2)	m_B (3)	m_V (4)	m_R (5)	m_I (6)	$U-B$ (7)	$B-V$ (8)	$V-R$ (9)	$R-I$ (10)
1	14.23 ± 0.32	14.83 ± 0.34	14.80 ± 0.36	14.64 ± 0.36	14.55 ± 0.39	-0.60 ± 0.66	0.03 ± 0.71	0.16 ± 0.73	0.09 ± 0.75
2	15.66 ± 0.31	16.45 ± 0.37	16.39 ± 0.43	16.19 ± 0.44	16.14 ± 0.50	-0.79 ± 0.68	0.06 ± 0.79	0.20 ± 0.85	0.05 ± 0.94
3	17.01 ± 0.56	17.75 ± 0.62	17.68 ± 0.68	17.44 ± 0.65	17.30 ± 0.68	-0.74 ± 1.19	0.06 ± 1.28	0.24 ± 1.30	0.14 ± 1.34
4	16.06 ± 0.08	16.64 ± 0.94	16.63 ± 0.95	16.50 ± 0.95	16.37 ± 0.96	-0.58 ± 1.86	0.01 ± 1.89	0.14 ± 1.90	0.13 ± 1.91
5	18.39 ± 0.43	19.21 ± 0.47	19.11 ± 0.53	18.78 ± 0.52	18.66 ± 0.59	-0.82 ± 0.90	0.09 ± 0.99	0.33 ± 1.06	0.12 ± 1.11
6	19.01 ± 0.32	19.63 ± 0.39	19.68 ± 0.43	19.24 ± 0.43	19.57 ± 0.60	-0.62 ± 0.72	-0.05 ± 0.83	0.45 ± 0.86	-0.33 ± 1.04
7	18.62 ± 0.44	19.45 ± 0.44	19.42 ± 0.43	19.38 ± 0.50	19.09 ± 0.51	-0.83 ± 0.88	0.03 ± 0.89	0.14 ± 0.96	0.15 ± 1.01
8	19.02 ± 0.79	19.32 ± 0.74	19.04 ± 0.78	18.71 ± 0.79	18.36 ± 0.82	-0.30 ± 1.54	0.28 ± 1.53	0.33 ± 1.57	0.35 ± 1.60
9	18.51 ± 1.05	18.87 ± 1.08	18.65 ± 1.09	18.43 ± 1.08	18.14 ± 1.11	-0.36 ± 2.13	0.22 ± 2.17	0.22 ± 2.17	0.29 ± 2.19
10	18.65 ± 0.66	19.38 ± 0.66	19.22 ± 0.66	18.82 ± 0.66	18.69 ± 0.70	-0.72 ± 1.22	0.16 ± 1.32	0.39 ± 1.32	0.23 ± 1.36
11	18.36 ± 0.44	19.18 ± 0.49	19.10 ± 0.51	18.75 ± 0.50	18.36 ± 0.51	-0.83 ± 0.93	0.08 ± 1.00	0.35 ± 1.00	0.39 ± 1.01
12	18.23 ± 0.50	18.66 ± 0.56	18.40 ± 0.56	18.17 ± 0.55	17.91 ± 0.60	-0.43 ± 1.06	0.25 ± 1.12	0.23 ± 1.12	0.26 ± 1.16
13	19.64 ± 1.08	19.91 ± 1.08	19.63 ± 1.10	19.31 ± 1.09	18.99 ± 1.11	-0.26 ± 2.16	0.27 ± 2.18	0.32 ± 2.19	0.32 ± 2.20
14	19.84 ± 0.60	20.15 ± 0.69	19.98 ± 0.71	19.33 ± 0.72	18.95 ± 0.74	-0.31 ± 1.20	0.17 ± 1.40	0.65 ± 1.43	0.38 ± 1.46
15	19.29 ± 0.66	19.49 ± 0.68	19.17 ± 0.70	18.90 ± 0.72	18.54 ± 0.73	-0.20 ± 1.33	0.32 ± 1.38	0.27 ± 1.41	0.35 ± 1.46
16	19.35 ± 0.71	19.83 ± 0.76	19.59 ± 0.73	19.32 ± 0.76	18.85 ± 0.73	-0.47 ± 1.47	0.24 ± 1.51	0.28 ± 1.51	0.47 ± 1.49
17	20.06 ± 0.71	20.50 ± 0.83	21.07 ± 0.89	20.66 ± 0.85	20.68 ± 0.96	-0.96 ± 1.54	-0.12 ± 1.72	0.41 ± 1.73	-0.02 ± 1.79
18	19.04 ± 0.80	19.43 ± 0.85	19.15 ± 0.85	18.89 ± 0.82	18.49 ± 0.83	-0.39 ± 1.63	0.28 ± 1.66	0.26 ± 1.66	0.40 ± 1.64
19	19.99 ± 0.79	20.64 ± 0.92	20.40 ± 0.93	20.00 ± 0.92	19.70 ± 0.96	-0.65 ± 1.71	0.25 ± 1.85	0.39 ± 1.85	0.30 ± 1.88
20	20.64 ± 1.13	20.99 ± 1.14	20.79 ± 1.18	20.33 ± 1.16	20.05 ± 1.19	-0.35 ± 2.27	0.20 ± 2.32	0.46 ± 2.33	0.29 ± 2.35
21	21.32 ± 0.53	21.72 ± 0.81	21.51 ± 0.92	21.08 ± 0.87	20.52 ± 0.87	-0.39 ± 1.33	0.21 ± 1.72	0.43 ± 1.79	0.56 ± 1.73
22	20.98 ± 1.12	21.16 ± 1.16	20.87 ± 1.18	20.80 ± 1.17	20.16 ± 1.11	-0.47 ± 2.27	0.29 ± 2.30	0.31 ± 2.32	0.41 ± 2.28
23	19.84 ± 0.94	20.35 ± 0.96	20.33 ± 1.04	20.12 ± 1.04	19.79 ± 1.03	-0.51 ± 1.90	0.02 ± 2.00	0.21 ± 2.06	0.34 ± 2.06
24	20.64 ± 1.12	21.07 ± 1.16	20.82 ± 1.17	20.56 ± 1.18	20.21 ± 1.16	-0.43 ± 2.29	0.26 ± 2.34	0.25 ± 2.35	0.35 ± 2.33
25	20.30 ± 1.06	20.54 ± 1.12	20.17 ± 1.12	19.92 ± 1.12	19.50 ± 1.09	-0.24 ± 2.19	0.37 ± 2.25	0.25 ± 2.25	0.41 ± 2.21

[1]Photometry within the apertures defined with the H_α frames. Cols. 2–6: magnitudes in the *UBVRI* Johnson bands; Cols. 7–10: colors. Data have been corrected from Galactic and inner extinction.

AGES AND MASSES

Table 22. Ages and Masses of knots in Mrk370

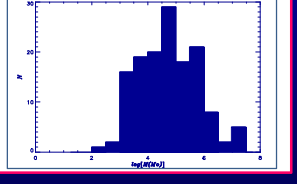
ID (1)	EW(Å) (2)	Age(Myr) (3)	$M(10^4 M_\odot)$ (4)	$U-B$ (5)	Age(Myr) (6)	$M(10^4 M_\odot)$ (7)
1	196.88	5.0	460	-0.59	5.6	530
2	333.97	5.0	120	-0.79	4.0	160
3	223.49	5.5	30	-0.74	5.0	32
4	81.02	6.5	81	-0.58	5.6	45
5	177.00	5.7	9.9	-0.82	4.8	6.5
6	260.73	5.6	7.3	-0.62	5.5	7.8
7	189.21	5.7	6.9	-0.83	4.8	4.5
8	96.81	6.3	11	-0.29	6.8	15.0
9	74.57	6.6	14	-0.36	6.6	17.0
10	123.56	6.2	9.6	-0.72	5.2	5.0
11	75.78	6.6	9.6	-0.82	4.8	3.0
12	49.05	7.2	15	-0.43	7.8	26.0
13	47.32	6.8	6.3	-0.26	6.7	6.9
14	79.68	6.5	4.7	-0.31	6.8	6.7
15	39.07	7.9	10	-0.50	...	...
16	62.01	6.9	4.9	-0.47	6.3	3.8
17	153.94	5.9	2.0	-0.85	4.8	1.1
18	28.84	8.4	1.1	-0.30	7.6	6.9
19	66.07	6.8	2.1	-0.64	5.4	0.83
20	71.51	6.7	1.7	-0.35	6.3	0.15
21	80.87	6.5	1.2	-0.42	6.2	0.10
22	58.48	7.0	1.4	-0.47	6.0	0.70
23	39.20	7.7	2.2	-0.51	5.8	0.57
24	39.92	7.9	1.5	-0.42	6.2	0.49
25	36.03	8.6	2.0	-0.23	...	...

[1]Col 1: Ids number as in Table6; Col 2: Ho Equivalent Width; Col 3: Age of each HII region calculated using the H_α equivalent width as age indicator; Col 4: Masses of each starburst region obtained using the previous parameter; Col 5: $U-B$; Col 6: Age of each HII region calculated using the $U-B$ color as age indicator. Col 7: Masses of each starburst region obtained using the previous parameter.

Table 30. Mean Ages

Galaxy (1)	$Z/Z_\odot$ (2)	$<Age(EW(H\alpha))>$ (3)	Δ_{age} (4)	$<Age(U-B)>$ (5)	Δ_{age} (6)	$C(H_\beta)$ (7)
Mrk370	0.5 [a]	6.6	0.9 [d]	5.9	0.9 [d]	0.26 [a]
Mrk600	0.1 [a]	5.5	4.0	4.7	1	0.20 [a]
IIZw40	...	...	...	...	...	...
Mrk5	0.2 [b]	...	...	5.5	1.3	0.42 [b]
IIZw71	0.2 [c]	7.9	6.0	6.1	3.1	...
Mrk297	0.4 [c]	5.8	0.5 [d]	5.3	0.3 [d]	0.41 [c]
IIIZw102	0.4 [c]	6.1	0.6 [d]	...	...	...
Mrk324	0.1 [c]	4.4	...	...	...	0.45 [c]
IIIZw107	0.2 [c]	6.1	1.2	...	...	...

[1]Column 2: Metallicity. Columns 3, 4: Averaged age of the knots and their age range derived with the $EW(H\alpha)$. Columns 5, 6: Idem but using the $U-B$ color as age estimator. Column 7: Internal reddening coefficients.
Notes.- [a] Cairós (2000); [b] Izotov et al. (1998); [c] Mazzarella et al. (1993).
[d] Assumed values, see text in Section 4.
[d] For *BCDs* with No. of knots catalogued ≥ 25, instead of Δ_{age} the σ value of the age distribution is provided.



By means of the EW(Ha) and the color U-B of the knots, and the STARBURST99 models, we derived the age and the mass of the exciting clusters. Results:

1. Data are consistent with an instantaneous star-formation law, with a Salpeter IMF (α=2.35) and a ranges of masses between ($1 \leq M/M_O \leq 100$).
2. In general there is a good agreement between both estimators
3. The mean age for the knots is ~5.0-6.5 Myr, implaying a coeval event
4. No differences are found in the four morpholycal classes except for IIZw71
5. The mass distribution ranges from ~10^2-10^4 M_O and peaks at about 10^5 M_O

Ha photometry observations

1. 2.5m NOT - instrument: ALFOCS 0.188 "/pixel
2. 2.2m CAHA - instrument: CAFOS 0.53 "/pixel
3. 1.5 m PO - instrument: CCD#13 0.378" /pixel

Broad band photometry observations

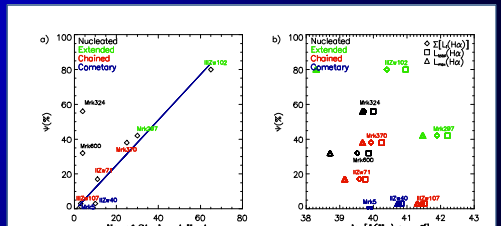
1. 2.5m NOT - instrument: ALFOCS 0.188 "/pixel
2. 2.2m CAHA - instrument: CAFOS 0.53 "/pixel

Mrk 370 is representative of the group of the Chained BCDs (Cairós et al. 2001b) in which 25 star-forming regions were identified, placed in a privileged direction that crosses the galxy from the northeast to the southwest. The brightest and the most massive regions are populating the optical center of the galaxy, where the surface brightness is about 1 or 2 orders of magnitude lager than in the rest of regions.

The Ha images were used for every galaxy for finding the star-forming regions. For measuring the star-bursting knots and generate the catalogues we used the IRAF package called *FOCAS*.

The knots identified in Ha are also measured in broad band, using the apertures defined with the Ha frames.

DIFFUSE EMISSION



Diffuse light emission (Ψ) shows a tendency in which BCDs with more star-forming knots have higher diffuse light fraction. Nevertheless, the Nuclated BCDs although having a few emission knots, present a high diffuse light content

Cometary BCDs are galaxies with practically no diffuse light, perhaps as a result of the compactness imposed in their ISM as they ram into the IGM

No correlation between the mean luminosity of the knots or the total luminosity of the galaxy and Ψ have been found

REFERENCES

Cairós, L.M., Vílchez, J.M., González-Pérez, J.N., Iglesias-Páramo, J., Caon, N. 2001a, ApJS, 133, 321

Cairós, L.M., Caon, N., Vílchez, J.M., González-Pérez, J.N.,Muñoz-Tuñón, C. 2001b, ApJS, 136, 393

Cairós, L.M., Caon, N., García-Lorenzo, B., Vílchez, J.M., Muñoz-Tuñón, C. 2002, ApJ, 577, 164

Kunth, D., Sargent, W.L.W., 1986, ApJ, 300, 496

Loose, H.H., Thuan, T.X., 1986, in Star Forming Dwarf Galaxies and Related Objects, 73

Papaderos, P., Loose, H.H., Fricke, K., Thuan, T.X. 1996, A&A, 314, 59

Sargent, W.L.W., Searle, L. 1970, ApJ, 162, L155

Telles, E. 1995, 1995, PhD Thesis

Thuan, T.X., Martin, G.E. 1981, ApJ, 247, 823